Study of the Noise Reduction Algorithm with Median Modified Wiener Filter for T2-weighted Magnetic Resonance Brain Images

Donghyeok Choi[1], Seong-Hyeon Kang[1], Chan Rok Park[2], and Youngjin Lee[1]*

[1]*Department of Radiological Science, Gachon University, 191, Hambakmoero, Yeonsu-gu, Incheon, Republic of Korea*
[2]*Department of Radiological Science, Jeonju University, 303, Cheonjam-ro, Jeonju-si, Jeollabuk-do, Republic of Korea*

The purpose of this study was to confirm the utility of the median modified Weiner filter (MMWF) noise reduction algorithm in T$_2$-weighted brain MR images. We acquired brain MR images using both real experiment and simulation, and performed comparative evaluation with conventional noise reduction algorithms through calculation of factors for the noise level and similarity. As a result, evaluation of the noise level and similarity showed the most improved in the image, which the MMWF noise reduction algorithm was applied. Moreover, additional experiment was conducted using real MR device and water phantom to more clearly prove the efficiency of the MMWF noise reduction algorithm. The noise level and intensity profile results derived from the real T$_2$-weighted MR image proved the effectiveness of the MMWF noise reduction algorithm. In conclusion, the proposed MMWF noise reduction algorithm demonstrated a very promising performance for improving the image quality in T$_2$-weighted MR image.

1. Introduction

Magnetic resonance imaging (MRI) can create a three-dimensional (3D) images by measuring the pattern, in which the atomic nuclei of hydrogen interact with the magnetic field and absorb and emit electromagnetic waves of a specific frequency without the risk of radiation exposure [1-4]. Then, acquired MR images were reconstructed to cross-sectional for the clinical diagnosis of lesions in the patient's body [5-7]. However, white noise with Gaussian distribution was occurred likewise other medical images when acquisition of MR images. The main cause of Gaussian noise added to MR images is thermal noise due to object for imaging, coil of MR devices, and signal interference from various electronic component [8]. MR images were reconstructed by inverse discrete Fourier transform for raw data. Because linearity and orthogonality of Fourier transform, real and imaginary channels in k-space are affected by uncorrelated Gaussian distribution with the same variance and zero mean [9].

Then, MR images with complex values are converted to magnitude and phase images with nonlinear operation, and this process changes the probability density function (PDF) of the MR images data. The signal intensity of MR images was calculated using two independent Gaussian variables and follows the Rician distribution [10]. The generated noise deteriorated the image characteristics of the MR images, thus degrading the accuracy of the diagnosis. To address this problem, various software-based noise reduction algorithms have been proposed. Many studies have investigated noise reduction using conventional algorithms with the median, Gaussian, and Wiener filters [11-14]. However, the main limitation of the above-mentioned conventional noise reduction algorithms is that information about the boundary line is lost due to a decrease in sharpness caused by blurring effect, which arises when the noise generated in multiple pixels is continuously removed. On the other hand, various studies on the latest techniques such as non-local means, wavelet transform, and deep learning algorithm to improve the noise problem of MR images are actively being conducted. However, the above-mentioned techniques have the disadvantages of requiring time resolution, control over many parameters, and a large amount of

data, respectively.

To address this issue, the noise reduction technology a median modified Wiener filter (MMWF) noise reduction algorithm was proposed by Cannistraci *et al.* in 2009 [15]. This algorithm was used to restore a deteriorated image by minimizing the average error and not reflecting the high-frequency noise outliers by applying median values during Wiener filtering [16, 17]. Especially, the MMWF noise reduction algorithm can fast image processing based on simple formula for calculation. In addition, the users can easily adjust the smoothing of the images due to it only has one parameter (i.e., kernel size) even if they have little or no professional knowledge related to image processing. To replicate the image acquisition protocols of MRI scanners, simulation tools that can create the image acquisition conditions are being developed. In particular, in the case of MR images, the MATLAB-based MRiLab simulation program that can easily set various variables and sequences and acquire images without motion artifacts has been developed [18]. The developed MRiLab simulation program facilitates straightforward research, and images can be compared and analyzed by changing various parameters. In particular, T_2-weighted images can be evaluated to identify lesions, such as at bleeding sites and during tumor screening [19-21].

Therefore, in this study, the usefulness of the MMWF noise reduction algorithm was evaluated using images, which acquired through MRiLab simulation program and real MR device. In addition, the signal-to-noise ratio (SNR), coefficient of variation (CV), and contrast-to-noise ratio (CNR) were calculated to quantitatively evaluate the noise level, while the correlation coefficient (CC) and universal quality index (UQI) were determined for similarity evaluation. In addition, the intensity profile was extracted to evaluate the pixel fluctuations in the image. The performance of the proposed algorithm was compared with that of the median, Gaussian, and Wiener filters.

2. Materials and Methods

2.1. Acquiring of simulated T_2-weighted brain images

Simulated T_2-weighted brain image was generated using the MRiLab simulation program. The imaging parameters were the following: a spin echo (SE) pulse sequence with flip angle (FA) = 90°, bandwidth = 80 kHz, slice thickness = 6 mm, field of view = 160 × 200 mm², matrix size = 640 × 800, and TR/TE = 10000/50 ms. Then, we added the Gaussian noise (i.e., amplifier noise) to the T2-weighted image acquired for modeling the deteriorated image. Generally, since MR images are affected by Rician

noise, modeling of Gaussian noise with a single variance value is inappropriate. Thus, degradation images were obtained by adding Gaussian noise with various variance values in this study. PDF of Gaussian noise is defined as follows [22, 23]:

$$N_g(z) = \frac{1}{\sqrt{2\pi\hat{\sigma}}} e^{-\frac{(z-\mu_{pdf})^2}{2\sigma_{pdf}^2}}, \tag{1}$$

Here, z represents the gray level, and μ_{pdf} and σ_{pdf}^2 the mean and variance value of random variable z, respectively. Based on above equation, we modeled Gaussian noise with variance values of 0.001, 0.005, 0.01, 0.05, and 0.1, which mean value 0 is applied, from the T_2-weighted image. Fig. 1 shows the deteriorated images and region of interest (ROI) set for quantitative evaluation.

2.2. Modeling of the MMWF noise reduction algorithm

The median filter, which is a conventional noise reduction algorithm, has the disadvantage of poor spatial resolution, while a Wiener filter has the problem of low efficiency of noise removal [24]. To compensate for these disadvantages, a MMWF noise reduction algorithm was modeled. This approach applies a noise reduction method based on the Wiener filter. The Wiener filter b_w is defined as:

$$b_w(x, y) = \mu \frac{\sigma^2 - v^2}{\sigma^2} + (p(x, y) - \mu), \tag{2}$$

where $b_w(x, y)$ is the output pixel value at location $p(x, y)$, μ and σ^2 are the mean and variance of the Gaussian noise in the image, v^2 is the noise variance of the mask matrix, and $x \times y$ is the size of the neighborhood area in the mask. The modification in the Wiener filter concerns the local mask mean around each pixel μ. This value is replaced with the local kernel median around each pixel equation image. In the MMWF noise reduction algorithm, a pixel signal is processed as an intermediate value instead of an average value. The functional of the MMWF noise reduction algorithm b_{mmwf} is defined as:

$$b_{mmwf}(x, y) = \tilde{\mu} + \frac{\sigma^2 - v^2}{\sigma^2}(p(x, y) - \tilde{\mu}), \tag{3}$$

where $b_{mmwf}(x, y)$ is the output pixel value at location $p(x, y)$, $\tilde{\mu}$ is the median value, which is used instead of the mean value in the Wiener filter. This equation calculates MMWF noise reduction filter with nonlinear spatial domains. By listing the signal strength of the pixels and using the median value, the effect of the outliers can be
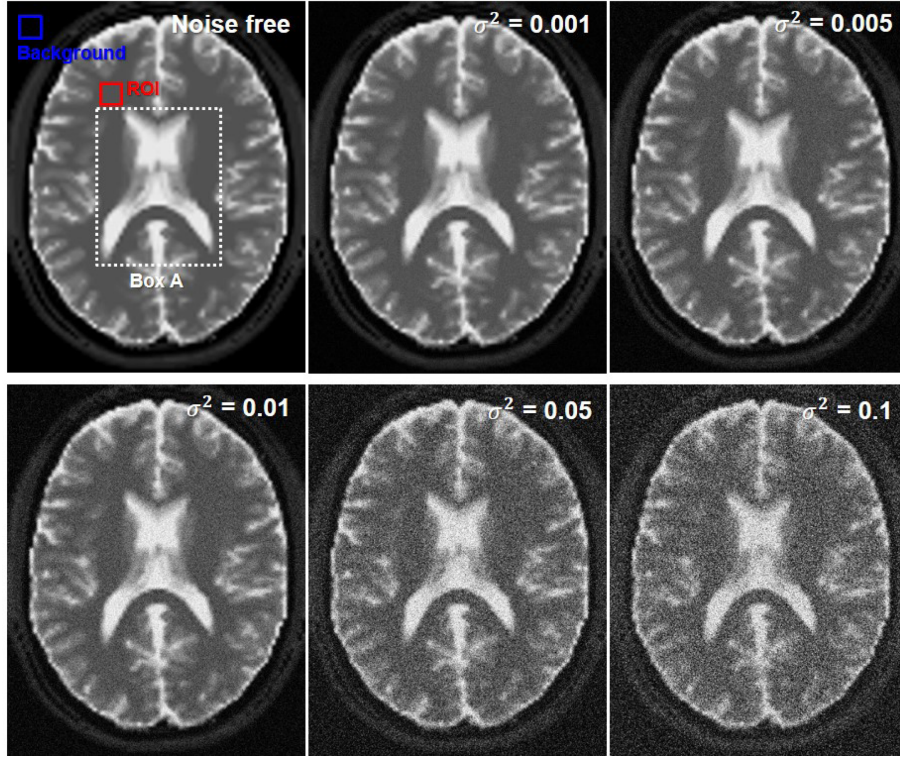
Fig. 1. (Color online) The deteriorated images, which Gaussian noise added with various variances (values: 0.001, 0.005, 0.01, 0.05, and 0.1) using MATLAB program.

minimized.

2.3. Quantitative evaluation of image characteristic

To evaluate the noise level of the image, the SNR, CV, and CNR of each image were calculated [25]. The SNR and CV are quantitative metrics for evaluating the noise in an image, while the CNR measure the difference in signal between two relevant structures in the image. The SNR, CV, and CNR are calculated as:

$$SNR = \frac{S_A}{\sigma_B}, \tag{4}$$

$$CV = \frac{\sigma_A}{S_A}, \tag{5}$$

$$CNR = \frac{|S_A - S_B|}{\sqrt{\sigma_A^2 + \sigma_B^2}}, \tag{6}$$

where S_A and S_B are the mean values in the ROI and background, respectively, and σ_A and σ_B are the standard deviations of the ROI and background, respectively. Among these factors, the CNR should be calculated by ROIs in two adjacent tissues. However, in the simulated T_2 weighted MR images, an effective ROIs could not be established due to the small white matter region. There-

fore, in this study, the background is set as the air region (Fig. 1).

2.4. Similarity evaluation of image characteristics

To evaluate the similarity of the reconstructed image to the original image, the CC and UQI were calculated. The CC measures the similarity between two images in terms of the Pearson autocorrelation coefficient. The UQI represents the linear correlation between two images, and it measures the similarity in the intensities of the two compared images. The closer the value of each factor is to 1, the higher is the similarity between the two images. The CC and UQI are calculated as follows:

$$CC = \frac{\Sigma_{p=1}^{N}(f_p - \bar{f})(g_p - \bar{g})}{\Sigma_{p=1}^{N}(f_p - \bar{f})^2 \Sigma_{p=1}^{N}(g_p - \bar{g})^2}, \tag{7}$$

$$UQI(f, g) = \frac{4\mu_f \mu_g \sigma_{fg}}{(\mu_f^2 + \mu_g^2)(\sigma_f^2 + \sigma_g^2)}, \tag{8}$$

where N is the number of image pixels; f_p is the original image; g_p is the restored image; $\bar{f}$ and $\bar{g}$ are the average pixel values of each corresponding image; μ_f and μ_g are the average of the signal intensity; σ_f and σ_g are the standard deviations, respectively, and σ_{fg} is the covariance

between the two images.

3. Results and Discussion

Brain lesions and tumor tissues contain a large amount of water. In T_2-weighted MR images, as most of the lesions appear as high-intensity signals, these images are often used to diagnose lesions. To accurately diagnose lesions, maintaining sharpness while reducing noise is important. The MRiLab simulation program can generate images similar to those acquired with a MRI scanner. In addition, the simulated images can be modeled using the MATLAB program, and various algorithms can be applied to improve the image characteristics. Therefore, in this this study, the deteriorated image was modeled based on the simulated T_2-weighed MR image, and the proposed MMWF noise reduction algorithm was applied to evaluate its utility.

We applied the conventional noise reduction algorithms and MMWF noise reduction algorithm in deteriorated images, which Gaussian noise with various variance values added, and the kernel size of each noise reduction algorithm was set to 5×5. Fig. 2 shows the noisy image (without algorithm applied) and reconstructed magnified images corresponding to the region in box A in Fig. 1. Quantitative evaluation factors were used to confirm the improvements in the image characteristics. Fig. 3 shows the results of the measured SNR, CV, and CNR of the reconstructed images obtained with each algorithm applied to the deteriorated images. The quantitative evaluation factors were measured based on the T_2-weighted brain image simulated with the MRiLab simulation program. The ROI set for evaluation is shown in Fig. 1.

The average SNR values of the noisy, median filter, Wiener filter, Gaussian filter, and MMWF noise reduction algorithm were calculated about 7.14, 17.15, 20.57, 11.06,
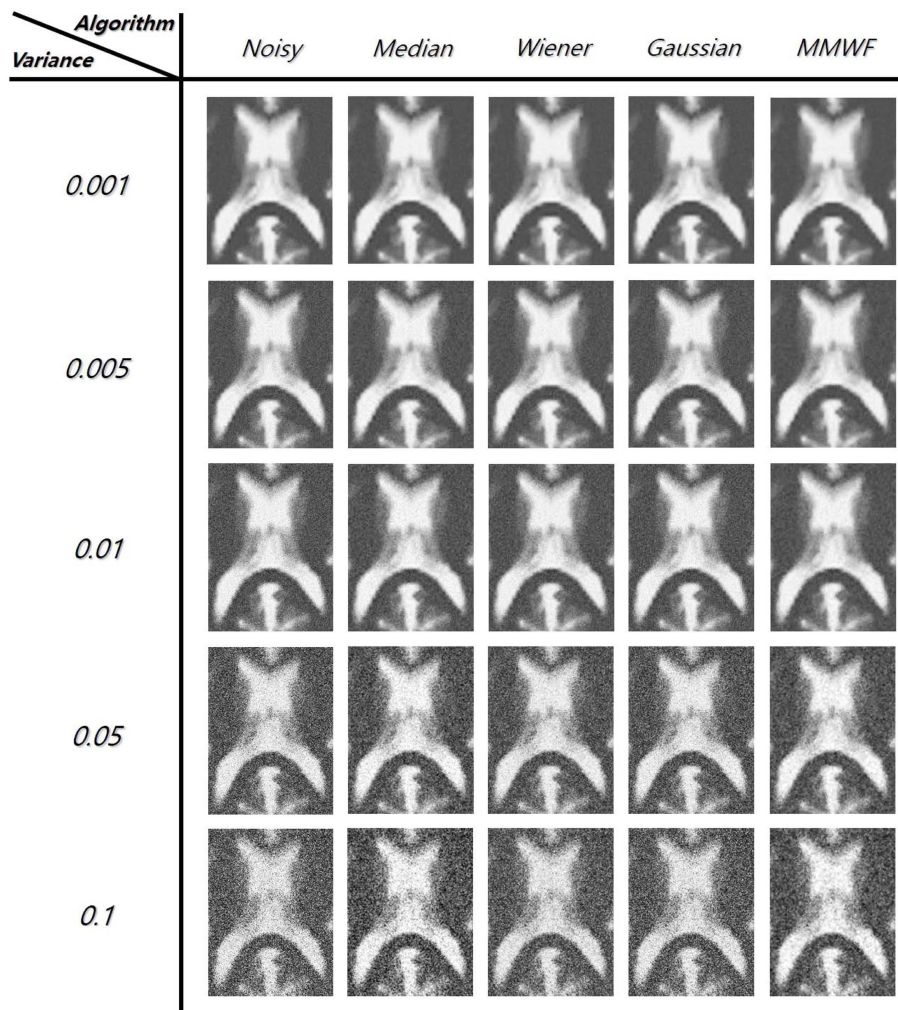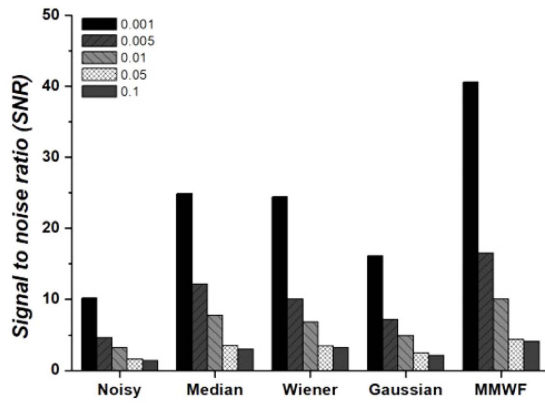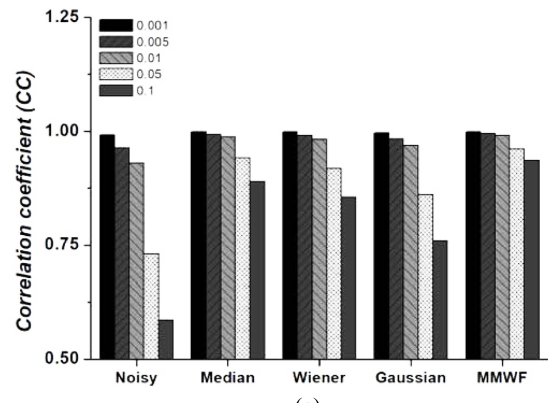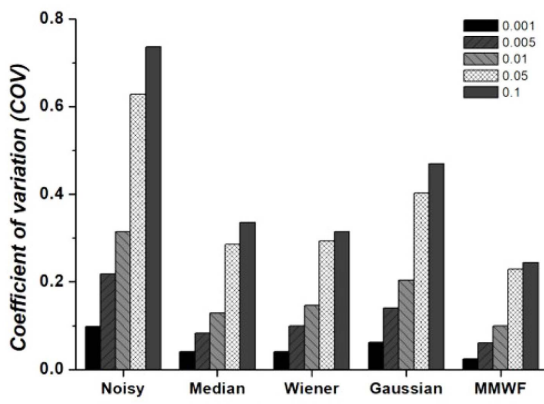

Fig. 2. Application of the conventional noise reduction algorithms and proposed MMWF noise reduction algorithm in deteriorated images.

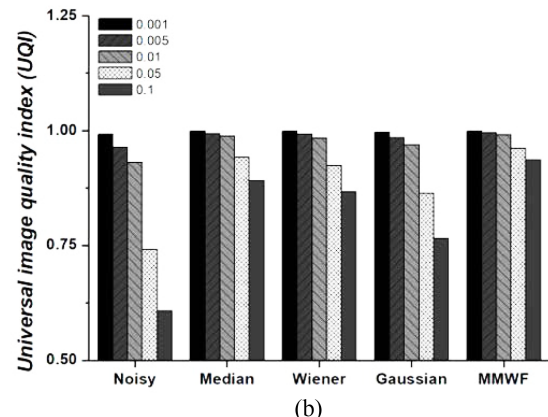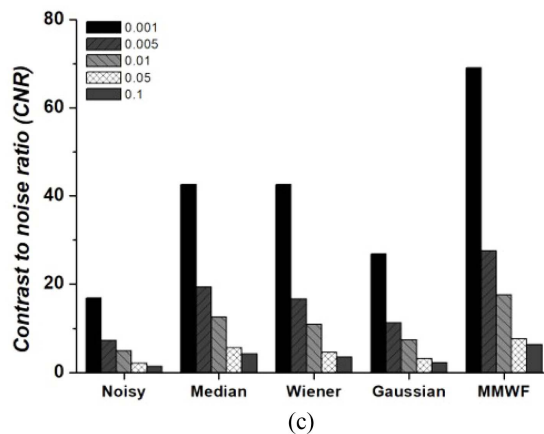Fig. 3. Results of the (a) signal-to-noise ratio (SNR), (b) coefficient of variation (CV), and (c) contrast-to-noise ratio (CNR) for reconstruction images using noisy, median filter, Wiener filter, Gaussian filter, and proposed MMWF noise reduction algorithm in simulated images, which Gaussian noise added with various variances (values: 0.001, 0.005, 0.01, 0.05, and 0.1).

and 27.03, respectively. The SNR results showed improvement in the order of the noisy, Gaussian filter, Wiener filter, median filter, and MMWF noise reduction algorithm. In particular, it was confirmed that the average

Fig. 4. Results of the (a) correlation coefficient (CC) and (b) universal quality index (UQI) for reconstruction image using noisy, median filter, Gaussian filter, Wiener filter, and proposed MMWF noise reduction algorithm in simulated images, which Gaussian noise added with various variances (values: 0.001, 0.005, 0.01, 0.05, and 0.1), compared to original image.

SNR value of the MMWF noise reduction algorithm applied image was improved by about 3.81, 1.47, 1.68, and 2.54 times compared to the noisy, median filter, Wiener filter, and Gaussian filter images, respectively. In addition, average CV values of the noisy, median filter, Wiener filter, Gaussian filter, and MMWF noise reduction algorithm were calculated about 0.40, 0.17, 0.18, 0.26, and 0.13, respectively. The CV results showed improvement in the order of the noisy, Gaussian filter, median filter, Wiener filter, and MMWF noise reduction algorithm. In particular, it was confirmed that the average CV value of the MMWF noise reduction algorithm applied image was improved by about 3.30, 1.38, 1.47, and 2.11 times compared to the noisy, median filter, Wiener filter, and Gaussian filter images, respectively. Moreover, average CNR values of the noisy, median filter, Wiener filter, Gaussian filter, and MMWF noise reduction algorithm were calculated about 6.48, 16.84, 15.63, 10.16, and

25.63, respectively. The CNR results showed improvement in the order of the noise, Gaussian filter, median filter, Wiener filter, and MMWF noise reduction algorithm. In particular, it was confirmed that the average CNR value of the MMWF noise reduction algorithm applied image was improved by about 3.97, 1.47, 1.68, and 2.54 times compared to the noisy, median filter, Wiener filter, and Gaussian filter images, respectively. The best SNR and CV, which evaluate the noise level, and CNR, which corresponds to the contrast, were obtained for the image reconstructed with the MMWF noise reduction algorithm.

Fig. 4 shows the results of the measured CC and UQI based on the T_2-weighted brain image simulated with the MRiLab simulation program. The average CC values of the acquired original simulated image (i.e., noise free image) and those obtained with the noisy, median filter, Wiener filter, Gaussian filter, and MMWF noise reduction algorithm were 0.84, 0.96, 0.95, 0.91, and 0.98 respectively (p-value < 0.05). The best results were obtained for the image reconstructed with the MMWF noise reduction algorithm. Especially, the CC values of the image with MMWF noise reduction algorithm improved by approximately 1.20, 1.02, 1.03, and 1.08 times compared with the noisy, median filter, Wiener filter, and Gaussian filter images, respectively. The corresponding average UQI values were 0.85, 0.96, 0.95, 0.92, and 0.98, respectively. Especially, the UQI values of the image with MMWF
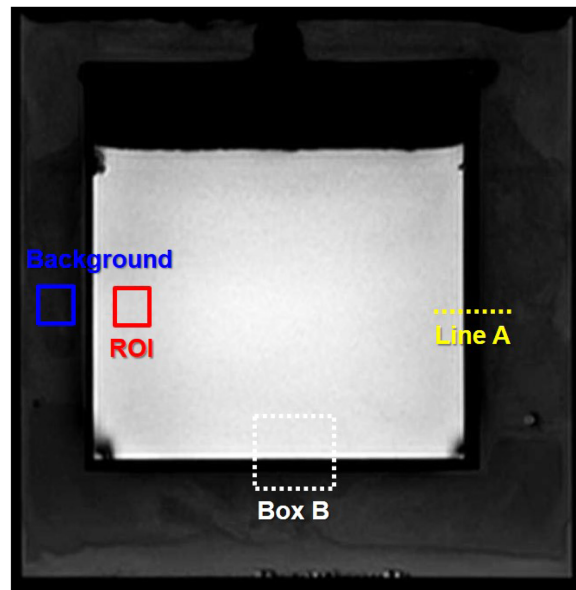

Fig. 5. (Color online) The real T_2-weighted MR image for water phantom with set ROIs for visual assessment and quantitative evaluation of image quality.

noise reduction algorithm improved by approximately 1.19, 1.02, 1.03, and 1.07 times compared with the noisy, median filter, Wiener filter, and Gaussian filter images, respectively. Both factors used for similarity evaluation indicated the superior performance of the MMWF noise
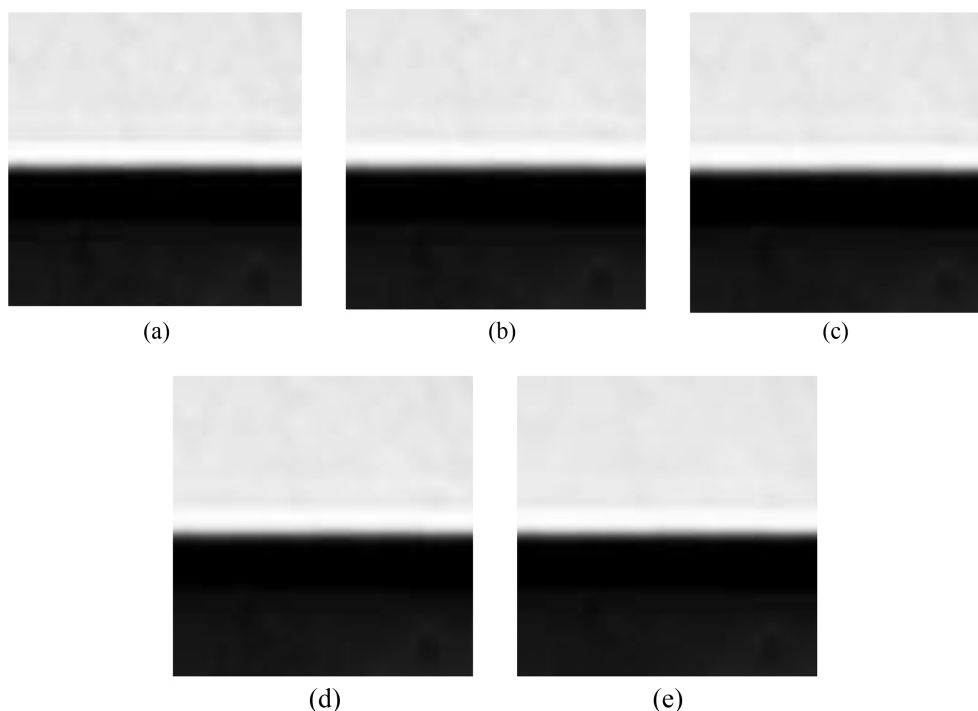

Fig. 6. Enlarged images of Box B in Fig. 5 of the T_2-weighted MR image for the water phantom using the noise reduction algorithms: (a) Noisy, (b) median filter, (c) Wiener filter, (d) Gaussian filter, and (e) MMWF noise reduction algorithm.
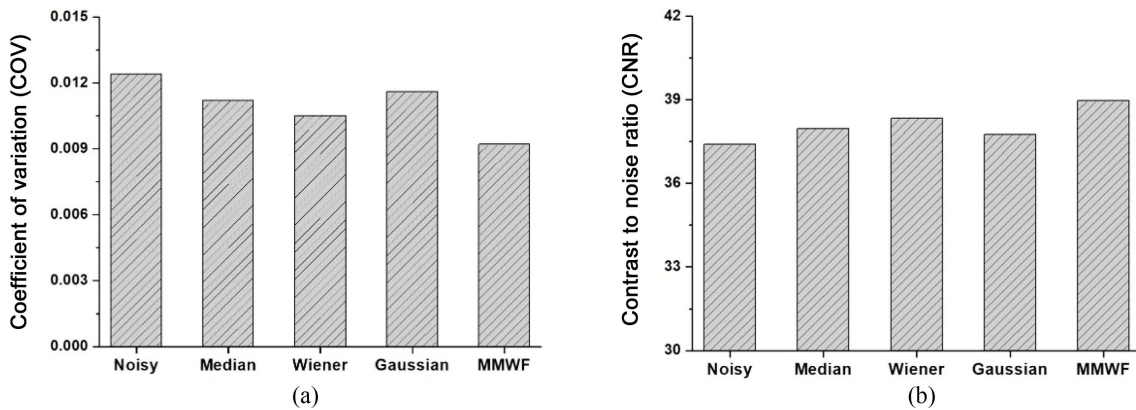
Fig. 7. Results of the coefficient of variation (CV) and contrast to noise ratio (CNR) for real T$_2$-weighted MR images with noise reduction algorithms.

reduction algorithm.

To clearly demonstrate the effectiveness of the MMWF noise reduction algorithm, further experiments were conducted using real MR device. To acquire the real T$_2$-weighted MR image, we used a real 3.0 T MR device (Philips Healthcare, the Netherlands) with water phantom. Then, the imaging parameters were the following: a spin echo (SE) pulse sequence with flip angle (FA) = 23°, slice thickness = 5 mm, field of view = 154 × 190, matrix size = 264 × 211, and TR/TE = 450/18.42 ms (Fig. 5). In addition, we applied the conventional noise reduction algorithms and proposed MMWF noise reduction algorithm to T$_2$-weighted MR images for water phantom. Fig. 6 shows the noisy image (without algorithm applied) and reconstructed images corresponding to the region in Box B in Fig. 5. Moreover, Fig. 7 shows CV and CNR were calculated for noise level analysis. The CV and CNR results showed improved results in the order of noisy, Gaussian filter, median filter, Wiener filter, and MMWF noise reduction algorithm. In particular, the CV and CNR of the MMWF noise reduction algorithm applied image showed improvements of approximately 1.35 and 1.04 times that of the noisy image.

Fig. 8 shows the intensity profiles of the images obtained by applying different filters to the deteriorated image. The intensity profile represents the signal intensity of each pixel in a region within a specified range. The intensity profile was measured based on the T$_2$-weighted image for water phantom. The range set for evaluation is shown in Fig. 5 intensity profiles along Line A. As indicated by the results, the image reconstructed with the MMWF noise reduction algorithm shows that the signal distortion on the boundary of the structures is reduced compared to conventional noise reduction algorithms.

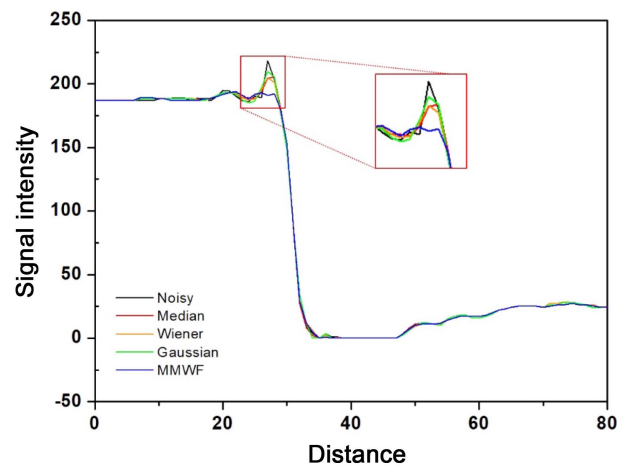Medical imaging is used an important basis for readings

Fig. 8. (Color online) Results of the intensity profile corresponding to Line A in Fig. 5: (a) Noisy, (b) median filter, (c) Wiener filter (d) Gaussian filter, and (e) proposed MMWF noise reduction algorithm, compared to T$_2$-weighted image for water phantom.

in the diagnostic process. However, the generated noise distorts, covers, and damages the information on the lesion, and provides inaccurate information about the anatomical details and boundaries. Because of these reasons, obtaining high-quality images through denoising is an indispensable requirement for examinations using the medical imaging system [26-28].

In order to solve the noise problem, various algorithms applied with the latest technologies have been proposed. In particular, the discrete Wavelet transform (DWT) [29], non-local means (NLM) [30], K-singular value decomposition (K-SVD) [31], and deep learning algorithms [32] have been actively studied recently, and show excellent performance in denoising. However, DWF and K-SVD have complex and many parameters that absolutely affect
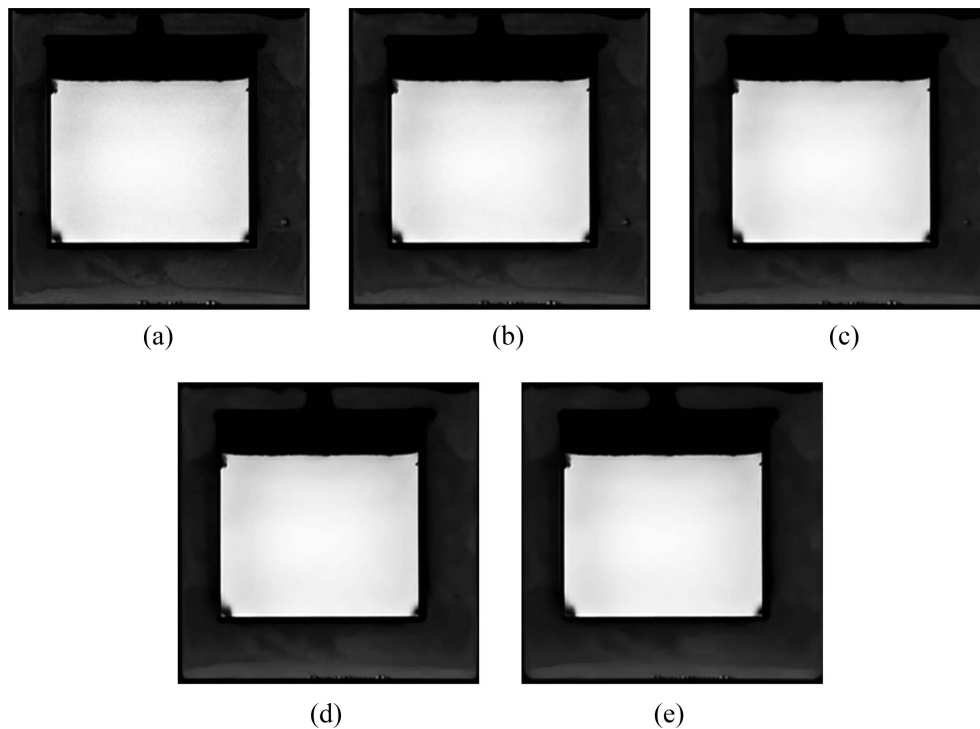
Fig. 9. The real T_2-weighted MR image with MMWF noise reduction algorithm, which was set each kernel size: (a) 3 × 3, (b) 7 × 7, (c) 11 × 11, (d) 15 × 15, and (e) 21 × 21.

denoising performance, and the setting of these parameters is subjective and empirical. In addition, NLM has limitations that application in medical and research fields due to inefficient operation time for estimating weights. Moreover, although deep learning-based algorithms require a large amount of training data to enhance effectiveness, it is difficult due to inappropriate environmental and ethical issue.

For these reasons, the latest technologies mentioned above have the disadvantage that it is difficult for ordinary users (i.e. students, non-major researchers, and radiologic technologist) to use them efficiently for their situation and purpose. Improperly applied denoising algorithms can lead to insufficient or excessive smoothing. In particular, excessive smoothing can be fatal for images with ambiguous distinctions between signals and noise, such as fMRI, which detects subtle changes in blood flow and measures brain activity [33]. In addition, a blurring effect
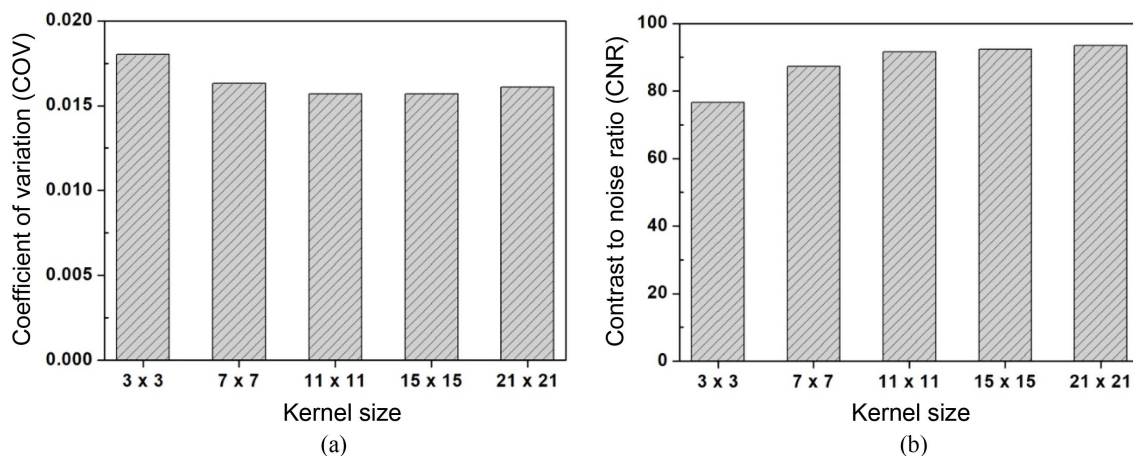

Fig. 10. Results of the coefficient of variation (CV) and contrast to noise ratio (CNR) for real T_2-weighted MR images with MMWF noise reduction algorithms, which were set each kernel size.

that causes distortion of the lesion and anatomical structure occurs [34].

Therefore, we modeled MMWF noise reduction algorithm, which is easy to handle and optimize due to a simple mechanism, and that can be applied immediately through fast operation time. The modeled MMWF noise reduction algorithm was applied from simulation and real MR images, and comparative evaluation was performed on the noise level and image restoration with conventional noise reduction algorithms. As a result, we confirmed that MMWF noise reduction algorithm is effectively applied regardless of the added noise level through simulation studies. Moreover, the feasibility of application from the clinical field was confirmed by applying MMWF noise reduction algorithm in real MR images.

However, as mentioned above, the application of an inappropriate algorithm effects as a factor that degrades the accuracy of the diagnosis. This means that optimization of the parameters of the algorithm is required. Therefore, we analyzed the tendency of image characteristics according to the change of kernel size, which the only parameter of the MMWF noise reduction algorithm by conducting further experiment. In order to perform further experiment, the kernel size of the MMWF noise reduction algorithm were set to 3×3, 7×7, 11×11, 15×15, and 21×21, respectively, and were applied to the real MR image. In addition, CV and CNR were measured to quantitative evaluate the noise level. Fig. 9 shows the real T_2-weighted images applied with the MMWF noise reduction algorithms, which were set each kernel size. In addition, Fig. 10 shows measured CV and CNR to analyze the noise level of T_2-weighted MR images according to the change of the kernel size for MMWF noise reduction algorithm. As a result, Fig. 10 shows that as the kernel size of the MMWF noise reduction algorithm increases, although the results of the noise-related evaluation factors improve, the degree decreases gradually. In addition, Fig. 9 shows as the kernel size increases, the image signal is gradually removed and the blurring effect is intensified. The results, which derived from further experiment, show that even if an algorithm that has been proven effective is applied from an MR image, the application of inappropriate parameters can degrade the image quality. Therefore, in the future, we intend to conduct a study on the optimization of the MMWF noise reduction algorithm for various conditions and purpose.

5. Conclusion

In this study, we evaluate the efficiency of the MMWF noise reduction algorithm in T_2-weighted MR images. For this purpose, a T_2-weighted MR images, which Gaussian noise added with various variance, were acquired using the MRiLab program. In addition, actual T_2-weighted MR images of the water phantom was acquired using real MR device. In conclusion, the proposed MMWF noise reduction algorithm demonstrated a very promising performance for improving the image quality in MRI, thus facilitating potential applications in current MRI technology.

References

[1] A. I. García-Díez, L. H. Ros Mendoza, V. M. Villacampa, M. Cózar, and M. I. Fuertes, Eur. Radiol. **10**, 462 (2000).

[2] R. Arkun, A. Memis, T. Akalin, E. E. Ustun, D. Sabah, and G. Kandiloglu, Skeletal Radiol. **26**, 167 (1997).

[3] Vijayalaxmia, M. Fatahi, and O. Speck, Research/ Reviews in Mutation Research **764**, 51 (2015).

[4] W. Hirsch, I. Sorge, S. Krohmera, D. Weber, K. Meier, and H. Till, Eur. J. Radiol. **68**, 278 (2008).

[5] C. A. Pelizzari, G. T. Chen, D. R. Spelbring, R. R. Weichselbaum, and C. T. Chen, J. Comput. Assist. Tomogr. **13**, 20 (1989).

[6] M. Takada, R. Kashiwagi, R. Sakane, F. Tabata, and Y. Kuroda, The American Journal of Emergency Medicine **18**, 192 (2000).

[7] R. Cox and A. Zesmanowicz, An Official Journal of the International Society for Magnetic Resonance in Medicine **42**, 1014 (1999).

[8] C. S. Anand and J. S. Sahambi, In TENCON 2008-2008 IEEE Region 10 Conference, 1 (2008).

[9] J. Yang, J. Fan, D. Ai, S. Zhou, S. Tang, and Y. Wang, Biomedical Engineering Online **14**, 1 (2015).

[10] J. Mohan, V. Krishnaveni, and Y. Guo, Biomed. Signal Process. Control **9**, 56 (2014).

[11] S. V. M. Sagheer and S. N. George, Biomed. Signal Process. Control **61**, 102036 (2020).

[12] L. Mredhula and M. A. Dorairangasamy, Int. J. Comput. Appl. **64**, 1 (2013).

[13] Z. Wang and D. Zhang, IEEE Transactions on Circuits and Systems II: Analog and Digital Signal Processing **46**, 78 (1999).

[14] A. M. Wink and J. B. T. M. Roerdink, IEEE Trans. Med. Imaging **23**, 374 (2004).

[15] M. Kazubek, IEEE Signal Process. Lett. **10**, 324 (2003).

[16] C. V. Cannistraci, F. M. Montevecchi, and M. Alessio, Proteomics **9**, 4908 (2009).

[17] T. J. Chen, K. S. Chuang, J. H. Chang, Y. H. Shiao, and C. C. Chuang, Journal of Digital Imaging **19**, 118 (2006).

[18] C. V. Cannistraci, A. Abbas, and X. Gao, Scientific Reports **5**, 1 (2015).

[19] F. Liu, R. Kijowski, and W. Block, Proc. Int. Soc. Magn. Reson. Med. **5244**, 4227 (2014).

[20] R. J. Ordidge, J. M. Gorell, J. C. Deniau, R. A. Knight, and J. A. Helpern, Magn. Reson. Med. **32**, 335 (1994).

[21] M. S. Shiroishi, G. Castellazzi, J. L. Boxerman, F. D'Amore, M. Essig, T. B. Nguyen, J. M. Provenzale, D. S. Enterline, N. Anzalone, A. D€orfler, A. Rovira, M. Wintermark, and M. Law, J. Magn. Reson. Imaging **41**, 296 (2015).

[22] H. M. Ali, High-Resolution Neuroimaging-Basic Physical Principles and Clinical Applications 111 (2018).

[23] N. Kumar and M. Nachamai, Oriental Journal of Computer Science and Technology **10**, 103 (2017).

[24] C. R. Park, S. H. Kang, and Y. Lee, Nuclear Engineering and Technology **52**, 2328 (2020).

[25] C. S. Anand and J. S. Sahambi, Magn. Reson. Imaging **28**, 842 (2010).

[26] E. Bergers, J. C. J. Bot, C. J. A. De Groot, C. H. Polman, G. J. Lycklama à Nijeholt, J. A. Castelijns, P. van der Valk, and F. Barkhof, Neurology **59**, 1766 (2002).

[27] J. Mohan, V. Krishnaveni, and Y. Guo, Biomed. Signal Process. Control **9**, 56 (2014).

[28] J. Rajan, J. Arnold, and J. Sijbers, Signal Process. **103**, 16 (2014).

[29] R. D. Nowak, IEEE Trans. Image Process. **8**, 1408 (1999).

[30] P. Coupé, P. Yger, S. Prima, P. Hellier, C. Kervrann, and C. Barillot, IEEE Trans. Med. Imaging **27**, 425 (2008).

[31] M. Aharon, M. Elad, and A. Bruckstein, IEEE Trans. Signal Process. **54**, 4311 (2006).

[32] M. Kidoh, K. Shinoda, M. Kitajima, K. Isogawa, M. Nambu, H. Uetani, K. Morita, T. Nakaura, M. Tateishi, Y. Yamashita, and Y. Yamashita, Magn. Reson. Med. Sci. **19**, 195 (2020).

[33] G. Strangman, J. P. Culver, J. H. Thompson, and D. A. Boas, Neuroimage **17**, 719 (2002).

[34] M. Mikl, R. Mareček, P. Hluštík, M. Pavlicová, A. Drastich, P. Chlebus, M. Brázdii, and P. Krupa, Magn. Reson. Imaging **26**, 490 (2008).